Journal of Biomolecular NMR, **24:** 15–30, 2002.
KLUWER/ESCOM

High resolution ^{13}C NMR spectra on oriented lipid bilayers: From quantifying the various sources of line broadening to performing 2D experiments with 0.2–0.3 ppm resolution in the carbon dimension

O. Soubias, O. Saurel, V. Réat & A. Milon*
Institut de Pharmacologie et de Biologie Structurale, IPBS CNRS, Pr A. Milon, 205 rte de Narbonne, 31077 Toulouse, France

Received 27 February 2002; Accepted 4 July 2002

Key words: B_0 field homogeneity, ^{13}C NMR, 2D J-resolved, membranes, mosaic spread, 2D PELF, J-resolved, shim, surface current

Abstract

^{13}C NMR spectra routinely performed on oriented lipid bilayers display linewidth of 1–2 ppm, although T_2 measurements indicate that 0.1–0.2 ppm could be obtained. We have prepared a DMPC – $^{13}C_4$-cholesterol (7/3) sample, and oriented the lipid bilayers between glass plates so that the bilayer normal makes an angle of 90° (or of the magic angle) with B_0. We have measured T_2s, CSAs, and linewidths for the choline ^{13}C-γ-methyl, the cholesterol-C_4 carbons and the lipid head group phosphorus, at both angles and 313 K. The magnetic field distribution within the sample was calculated using the surface current formalism. The line shapes were simulated as a function of B_0 field inhomogeneities and sample mosaic spread. Both effects contribute to the experimental linewidth. Using three signals of different CSA, we have quantified both contributions and measured the mosaic spread accurately. Direct shimming on a sample signal is essential to obtain sharp resonances and ^{13}C labelled choline methyl resonance of DMPC is a good candidate for this task. After optimisation of the important parameters (shimming on the choline resonance, mosaic spread of $\pm 0.30°$), ^{13}C linewidth of 0.2–0.3 ppm have been obtained. This newly achieved resolution on bilayers oriented at 90°, has allowed to perform two 2D experiments, with a good sensitivity: 2D PELF (correlation of carbon chemical shifts and C-H dipolar couplings) and 2D D-resolved experiment (correlation of carbon chemical shifts and C-C dipolar couplings). A C-C dipolar coupling of 35 ± 2 Hz between the choline methyl carbons was determined.

Introduction

Solid state NMR spectroscopy of oriented membrane samples provides a robust method for examining the structure, the dynamic and the orientation of membrane peptides (Cross, 1997; Marassi et al., 1997) or sterols (Marsan et al., 1999) and has emerged in recent years as a powerful technique to characterise structural constraints of small molecules at their binding sites within membrane proteins (Glaubitz et al., 1999; Williamson et al., 1998). Static spectra of isotopically labelled and uniaxially oriented samples are characterised by single line resonances in all frequency dimensions. Since the observed resonance frequencies depend on the orientation of the molecular sites relative to the magnetic field direction, they provide the orientational constraints used in structure determination. For instance, the orientation and the structure of a peptide in the membrane can been determined by ^{15}N labelling of the amides or ^{13}C labelling of the carbonyls in the peptide backbone (Bechinger et al., 1993; Separovic et al., 1994), the sterol order parameters can be extracted from quadrupole splittings of specifically deuterated positions (Dufourc et al., 1984). Bilayers mechanically oriented between glass plates thus provide an excellent model of natural

*To whom correspondence should be addressed. E-mail: alain.milon@ipbs.fr

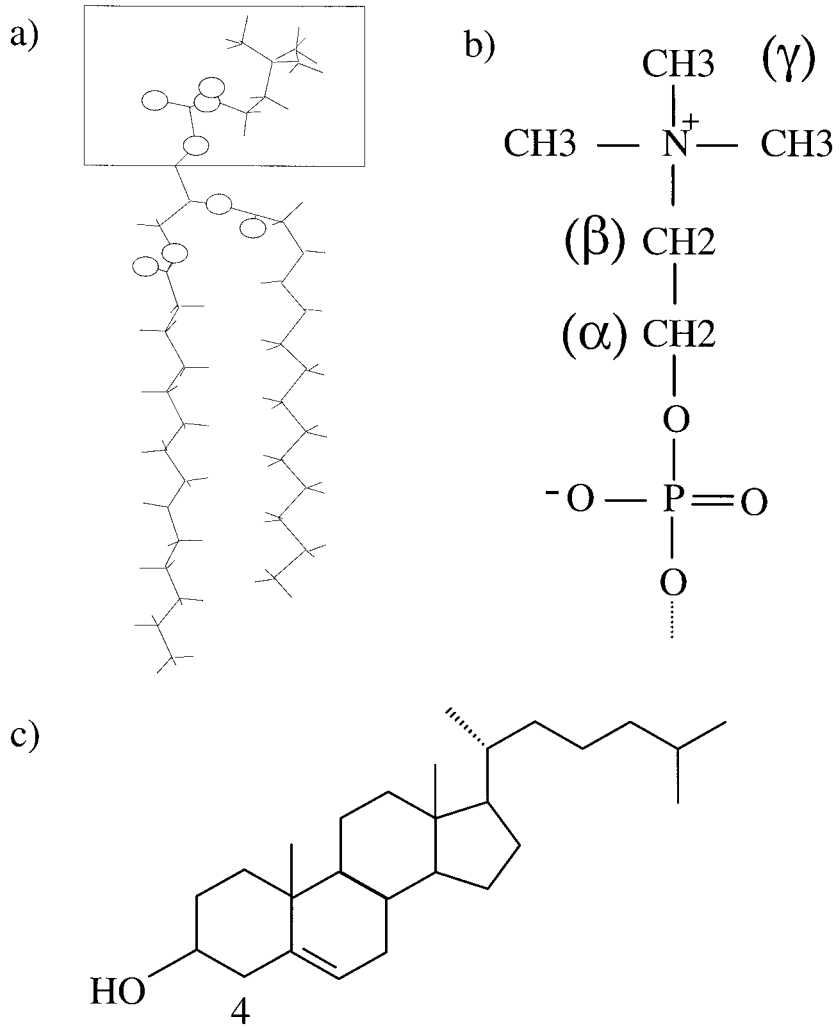

Figure 1. (a) DMPC, (b) choline polar head structure, and (c) cholesterol structure.

membrane. We have recently determined cholesterol order parameters in DMPC – $^{13}C_4$-cholesterol oriented bilayers from the C-H dipolar couplings using 2D PELF correlating ^{13}C chemical shifts and H-C dipolar coupling (Massou et al., 1999) identical to those previously obtained with deuterium NMR using specifically deuterated cholesterol (Marsan et al., 1999). However, in this experiment we systematically observed that cholesterol-C_4 resonance has an apparent linewidth (1.5 ppm) much larger than expected from its transversal relaxation time (T_2) from which we expect a refocused linewidth of 0.21 ppm. Resolution generally available on mechanically oriented samples is close to 1–2 ppm and it would be highly desirable to increase it by at least one order of magnitude.

The aim of the present study was to understand the different sources of carbon line broadening in these oriented samples and to determine how to improve the resolution in the ^{13}C spectra of oriented bilayer systems. We have specifically investigated the role of the sample geometry on B_0 field inhomogeneities both theoretically and experimentally, the contribution of the quality of sample orientation (extent of liposomes and mosaic spread). We have shown that direct shimming on a sample resonance makes it possible to obtain linewidth in the 0.1 ppm range and to perform new 2D NMR experiments on such oriented samples.

Materials and methods

Computation of induced magnetic field distribution

Magnetisation is induced in any material subjected to a strong uniform magnetic field $\mathbf{B_0}$ (term commonly applied to the magnetic flux density) and can be expressed as $\mathbf{M} = \frac{\chi \mathbf{B_0}}{\mu_0(1+\chi)}$, where χ is the material magnetic susceptibility and μ_0 the permeability of free space. The induced magnetisation then generates a field ($\mathbf{B_{ind}}$) which adds to and thereby distorts the original field $\mathbf{B_0}$. $\mathbf{B_{ind}}$ calculation can be simplified in the case where $\chi \ll 1$ (Barbara, 1994). Since $\mathbf{M}$ is typically four or five orders of magnitude smaller than $\mathbf{B_0}$ for all cases of interest, the local effects of $\mathbf{M}$ on $\mathbf{B_0}$ may be neglected in the calculation of $\mathbf{M}$. Thus, $\mathbf{M}$ may be assumed to be independent of the geometry of the material and replaced with an equivalent surface current $\mathbf{J}$ that is given by $(\mathbf{M_2} - \mathbf{M_1}) \wedge \mathbf{n}$, where $\mathbf{n}$ is a unit normal vector to the surface of the material and directed from region 2 to region 1 with uniform magnetisation $\mathbf{M_2}$ and $\mathbf{M_1}$, respectively (see Figure 8 for parameters definitions). Calculation of the induced magnetic field then requires the evaluation of surface integrals of the form:

$$\mathbf{B_{ind}}(\mathbf{r}) = \frac{\mu_0}{4\pi} \iint d^2\mathbf{r}' \frac{\mathbf{J}(\mathbf{r}') \wedge (\mathbf{r} - \mathbf{r}')}{(\mathbf{r} - \mathbf{r}')^{3/2}}$$

Theoretical details of the calculations are presented in Appendix A.

The induced field created in membrane sample has been calculated for three different models presented in Figure 2. The sample, i.e., glass plates and multilayers of lipids, is sandwiched between two cylindrical spacers, the whole system being surrounded by the tube. The exact magnetic susceptibility (χ) of the lipid bilayers is unknown but since water ($\chi_{water} = -9.05 \times 10^{-6}$) and alkanes have similar magnetic susceptibilities (e.g. $\chi_{hexane} = -7.10 \times 10^{-6}$), we took the value of water as a model for multilayers of water and lipids. Since χ difference between two media appears as a common factor in all B_{ind} equations (see Appendix A), it just weights the relative contribution of the facial and lateral induced fields, and small errors in χ values might change the absolute values in our simulations but not the general trends. Simulations were done using magnetic susceptibility of the spacers equal to the glass one (model 1 and 3) or to the air one (model 2). The diameter of the cylindrical arrangement was either adjusted to the interior diameter of the tube (model 1 and 2) or chosen smaller thus allowing space for a cylindrical air layer (model 3). Models 2 and 3 allow us to test the influence of large χ differences between lipids/glass stacking and the surrounding media in axial and radial directions, respectively.

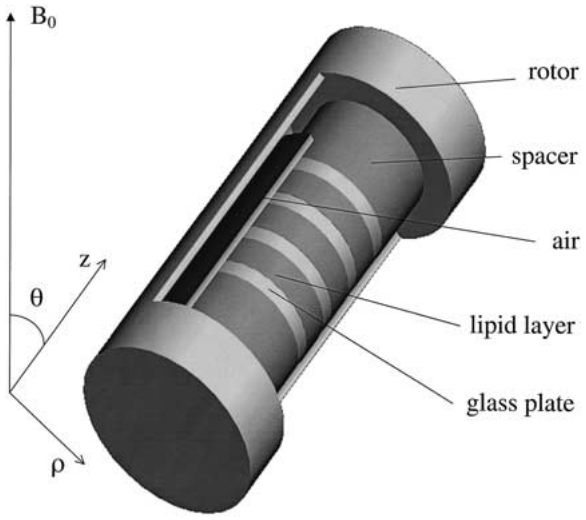

Figure 2. Geometry of the simulated oriented bilayer sample. Model 1 is constituted by 101 circular glass plates ($\chi = -11.8 \times 10^{-6}$), between which lays the sample ($\chi = -9.05 \times 10^{-6}$). The whole system is inserted into the Kel-F tube ($\chi = -11.6 \times 10^{-6}$). Glass spacers are present between the sample and the Kel-F tube caps. Model 2 differs from model 1 by an air volume ('spacer') between the sample and the rotor caps ($\chi = 0.03 \times 10^{-6}$). In Model 3, glass plates and the tube cylindrical wall are separated by a cylindrical air layer, the rest of the system being identical to Model 1. B_0 direction makes an angle $\theta = 90°$ with respect to the long sample z axis. Other values of θ, in particular θ = magic angle, were tested and did not modify significantly the results presented herein. The axis origin is chosen in the middle of the central sample layer (51^{st} layer). The magnetic susceptibility values were extracted from Doty et al. (1998).

Induced magnetic field intensities were calculated at various radial positions in the middle of each lipid layer. The variation as a function of z inside a single lipid layer has also been calculated for several radial positions and was shown to be very small as illustrated in Figure 3d. Note that the B_{ind} calculations have not been performed very close to the lipid layer/glass and lipid layer/tube interfaces for which the convergence of Romberg integrations becomes time consuming. The volume explored by the simulation represented 90% of the total volume and the remaining 10% of the sample was shown to have no major contributions on the linewidths.

Line shape simulations

B_0 field inhomogeneity and mosaic spread contributions to the apparent linewidth have been simulated by the following way.

First, a lorentzian line of known T_2 was broadened by convolution with a Gaussian distribution of B_0 field defined by its standard deviation (σ'), giving the following line shape:

$$f(\omega) = \int_{-\infty}^{+\infty} \frac{1}{\sqrt{2\pi}\sigma} \exp\left[-\frac{1}{2}\left(\frac{\omega_0}{2\pi\sigma'}\right)^2\right] \cdot \frac{1}{\pi} \cdot \frac{T2}{1+(T_2\cdot[\omega-\omega_0])^2}\, d\omega_0.$$

This line is characterised by a half height linewidth called Δ' (in frequency unit), which is a function of both T_2 and σ'.

In order to also include mosaic spread broadening effect, we introduced a Gaussian distribution of angle θ around the mean value θ_0, with a standard deviation σ, thus giving the following line shape (valid for molecules with fast axial diffusion along the bilayer normal):

$$L(\omega) = \int_0^{3\sigma}\int_0^{2\pi} \frac{1}{\sqrt{2\pi}\sigma} \exp\left[-\tfrac{1}{2}\left(\tfrac{\theta}{\sigma}\right)^2\right] \cdot \frac{1}{\pi} \cdot \frac{\frac{1}{\pi\cdot\Delta'}}{1+\left\{\frac{1}{\pi\cdot\Delta'}\cdot\left(\omega-\left(\omega_\perp+(\omega_{//}-\omega_\perp)\cos^2\alpha\right)\right)\right\}^2} \cdot \sin\theta.d\varphi.d\theta,$$

where $\cos\alpha = \cos\theta\cos\theta_0 + \sin\theta\sin\theta_0\cos\varphi$. $\omega_\perp$ and $\omega_{//}$ are the resonance frequencies at $\theta_0 = 90°$ and $0°$ respectively. The CSA ($\omega_{//}-\omega_\perp$) is axially symmetric due to the fast axial diffusion of all molecules in the bilayer.

The final half height linewidth finally depends on T_2, the known transverse relaxation time of the resonance of interest, σ' the standard deviation characterising the Gaussian distribution of B_0 field, and σ, the standard deviation characterising the Gaussian distribution of bilayer orientations. We define the sample 'mosaic spread' as the value $\pm\sigma$ in degrees, i.e., the interval of orientation in which lays 68% of the sample. Note that whenever values were given in Hz, a 500 MHz spectrometer (125 MHz ^{13}C) has been assumed.

Synthesis of 1,2-dimyristoyl-sn-glycero-3-phospho-[γ-^{13}C]-choline (DMPC-[γ-^{13}C]) from 1,2-dimyristoyl-sn-glycero-3-phosphoethanolamine (DMPE)

DMPC labelled at the N-methyl position was synthesised from dry DMPE (1.57 mmol, Sygena lipids) by adding an excess of ^{13}C methyl-iodide (6.28 mmol, 412 μL, Euriso-top) and 1,8-diazabicyclo[5.4.0]undec-7-ene (6.28 mmol, 940 μL, Aldrich) in toluene (15 mL) at room temperature (reaction time 16 h). The permethylated product was purified according to the method described previously (Bersch et al., 1993), with an overall yield of 84%. The 1,2-dimyristoyl-sn-glycero-3-phospho-[γ−^{13}C]-choline was characterised by ^1H and ^{13}C NMR ($CDCl_3$). The ^1H chemical shifts were found to be the same as the non-labelled compound and carbon 13 spectrum ensured that permethylation of the ethanolamine polar head was complete. Mass spectrometric analysis with an ESI source (negative mode) gave an unique peak at m/z = 684.2 corresponding to the permethylated product.

Oriented bilayers

Oriented liquid crystalline samples were prepared from Small Unilamellar Vesicles (SUVs) suspensions composed of 8.1 mg DMPC-[γ−^{13}C]/1.4 mg $^{13}C_4$-cholesterol (70:30 mol%) in water and produced using a tip sonifier. The $^{13}C_4$-cholesterol was purchased from C.D.N. Isotopes, Inc. The vesicle suspension was spread onto the glass plates (Marienfeld Inc.), previously pickled overnight in fuming nitric acid, then rinsed carefully and dried 1 h at 80 °C. After solvent evaporation under vacuum, 5 cycles of dehydration–hydration (in water saturated atmosphere, at 40 °C) were applied to the sample. Before NMR experiments, the hydrated plates were stacked into the tube and the sample was equilibrated overnight at 40 °C.

For each sample, the lipid surface density was calculated to be 1 mg/cm^2. Forty coverslips (5.5 mm diameter, 70 μm thickness) were stacked in a KelF tube (7-mm outer diameter O.D., 25 mm long) for 2D static 90° experiments and 75 coverslips (3.8 mm diameter, 70 μm thickness) were stacked in a zircon MAS rotor (5 mm O.D.) for 1D 90° and magic angle experiments. The quality of orientation and hydration was controlled by ^{31}P NMR using the chemical shift anisotropy of the DMPC phosphate.

NMR experiments

The NMR experiments were performed on a DMX Bruker narrow bore spectrometer operating at 500 MHz for ^{1}H. All experiments were performed at 313 K. Proton-decoupled CP static ^{13}C spectra were acquired with a 2.5 msec contact time to enhance the lipids resonances or 0.5 msec to enhance the sterol resonances. The acquisition time was 40 ms (8K data points, dwell time 5 μs) and a repetition delay of 3s was used both for relaxation and for preventing sample heating. Static NMR spectra at 0° (rectangular glass plates) and 90° (circular glass plates) were recorded on a Bruker 7 mm double resonance probe, with a solenoid coil oriented at 90° with respect to the magnetic field. Magic angle experiment were performed on a Doty triple resonance 5 mm MAS XC5 probe. Linear prediction (8K points) without apodization function was used before Fourier transform.

The two-dimensional Proton Encoded Local Field (PELF) experiment (Caldarelli et al., 1996) was obtained with a 100 μs cross-polarisation contact time. A total of 128 t_1 increments (dwell time 91 μs) with 128 scans each were collected. MREV-8 ^{1}H decoupling at 66 kHz was applied during the evolution period, and 60 kHz TPPM (Bennet et al., 1995) was used during acquisition. Quadrature detection in t_1 dimension was achieved using the States method. The two dimensional ^{13}C 'D-resolved' experiment was acquired under constant proton decoupling reduced to a level sufficient to provide adequate decoupling for choline resonance while minimising sample heating and spin echo was maximal with a 5 μs carbon π pulse. A total of 64 t_1 increments (dwell time 500 μs) with 32 scans each were collected.

Processing parameters of 2D experiments included linear prediction in the indirect dimension (256 points), zero filling and standard apodization functions.

Results and discussion

Critical spectral parameters

Table 1 summarises the different values of chemical shift anisotropy and T_2 obtained for both lipid and sterol signals. The chemical structures of the corresponding molecules is shown in Figure 1. Carbon 13 NMR spectra of DMPC – $^{13}C_4$-cholesterol Multilamellar Vesicles (MLV) were recorded under slow magic angle spinning (MAS) conditions. We obtained the tensor element magnitude from analysis of the resultant spinning sideband pattern using the Herzfeld-Berger method (Herzfeld and Chen, 1996). The CSA values were also determined on bilayers oriented perpendicular and parallel to the magnetic field director. From both measurement an axially symmetric CSA was found as expected, since above the gel to liquid crystalline phase transition temperature, lipids undergo fast uniaxial motions along the bilayer normal. From previous analyses where a single deuterium and C-H dipolar splitting is observed for the three CH_3 groups in the $N^+(CH_3)_3$ moiety (Hong et al., 1995a,b; Seelig et al., 1977), it has been strongly suggested that a fast motion with at least C_3 symmetry occurs around the C_β-N bond. Moreover, extensive dynamics is expected to occur within the polar head. Such a motional behaviour explains that choline methyl tensor (~2 ppm, prolate) was found to be one order magnitude smaller than cholesterol methylene tensor (~20 ppm, oblate).

Table 1. Key spectral parameters measured for an oriented bilayer system composed of DMPC-Cholesterol (7:3 mol%). $\Delta\delta = \delta_{||} - \delta_{\perp}$: Chemical Shift Anisotropy. Due to the fast axial diffusion of all molecules in the liquid cristalline phase, all CSAs are axially symmetric. T_2 relaxation rates were determined in a spin echo experiment under continuous proton decoupling conditions. $1/\pi T_2$ (δ_{iso}): Transverse relaxation rate for bilayers oriented at the magic angle (angle between B_0 and the bilayer normal of 54.7°) converted into half height linewidth in ppm (1 ppm = 125 Hz). $1/\pi T_2$ ($\delta_{\perp}$): Transverse relaxation rate for bilayers oriented at 90° converted into half height linewidth

Nucleus	$\Delta\delta$ (ppm)	$1/\pi T_2$ (δ_{iso}) (ppm)	$1/\pi T_2$ ($\delta_{\perp}$) (ppm)
$^{13}C\gamma$-choline	2.0 ± 0.3	0.096 ± 0.005	0.120 ± 0.005
$^{13}C_4$-cholesterol	-20.0 ± 0.6	0.14 ± 0.01	0.21 ± 0.01
^{31}P-DMPC	48.0 ± 2	0.55 ± 0.03	ND

T_2 relaxation time with bilayer normal perpendicular to the magnetic field was measured with a spin-echo experiment for both carbon resonances. Fast spinning (up to 3 kHz) ^{31}P and ^{13}C spectra were recorded with bilayer normal oriented at the magic angle (Glaubitz and Watts, 1998) (MAOSS) to measure T_2 when $\delta = \delta_{iso}$. As already described in the literature (Dufourc et al., 1992; Watnick, 1990), the transverse relaxation is anisotropic and slightly different T_2 were found at 90° and magic angle. In both cases, the linewidth expected from these relaxation rates (0.1~0.2 ppm for carbon resonances, 0.55 ppm

for ^{31}P) were much smaller than the experimental linewidths usually found (1∼2 ppm). Clearly, these are limited by others factors.

Parameters affecting carbon 13 linewidth in oriented bilayer systems

B_0 field inhomogeneities. Variations of the relative induced magnetic field intensity (B_{ind}-$B_{ind,c}$)/B_0 are displayed in Figure 3a (simulation 1), b (simulation 2) and c (simulation 3). $B_{ind,c}$ is the value of the induced field obtained at the centre of the sample stacking. B_0 direction makes an angle $\theta = 90°$ with respect to the long sample z axis. For the first model, in which spacers with a χ equal to the glass's one have been put on both sides in the axial direction ('ideal sample'), one can see that the variations within the sample are negligible. On the other hand, variations deduced from simulation 2 and 3 are more important and present a different field shape. For model 2 (axial discontinuities in χ), the relative induced magnetic field intensity decreases regularly in z direction down to -3.2 ppm, while the deviation along the radial axis is less important. For model 3 (possessing a cylindrical air layer around the sample), the induced magnetic field intensity increases significantly only at the extreme z and ρ values, leaving the major central part of sample with variation of less than 0.1 ppm. The corresponding half height linewidths are similar for simulation 1 and 3 (0.10 and 0.11 ppm) and increase by a factor 7 for simulation 2 (0.71 ppm).

From comparison of the field shape obtained from model 2 and 3, one can see that magnetic susceptibility differences between the sample and the surrounding media are more critical in the z direction than in the radial direction. It shows that line broadening of the order of one ppm can be expected from induced fields effects and that practically one must pay the most attention to χ discontinuities along the main axis direction.

It is interesting to observe that the overall field shape varies in a smooth manner over the whole sample. Figure 3d shows that B_0 field variations within one multi-layer (10 μm thickness) are one order of magnitude smaller than the difference between two consecutive multi-layers. Therefore, it should be possible to correct for B_{ind} effects via careful shimming. This was confirmed by preparing a stack of glass plates and water layers and by shimming it on the water signal: a proton linewidth of 0.05 ppm could be obtained thus demonstrating that this sort of sample geometry is compatible with a fairly homogenous internal field. However, the shim parameters classically used for solid NMR experiment on oriented membranes are those obtained from shimming on an identical tube filled with water. Induced magnetic field created by a water tube (model 1 for which magnetic susceptibilities of sample and glass plate are equal to the water one) has been calculated (Figure 3e). The induced field variations are of opposite sign and with a shape different from those obtain for the models 1 and 2 (Figure 3a, b). Therefore the required corrections in order to get an homogeneous field for a water cylinder sample are not applicable for a glass/water stacking.

Even though these simulations use several approximations (perfect symmetrical sample, homogeneous external B_0 field, lipid magnetic susceptibility equal to that of water), these results suggest that induced field effects can be made negligible, provided that one uses an internal probe to shim directly on the sample to be analysed.

Quality of orientation: Liposomes and mosaic spread. Figure 4 shows a series of spectral simulation of ^1H-decoupled carbon NMR spectra of oriented or unoriented samples. Figure 4a represents the typical powder pattern spectrum observed with liposomes, i.e., a spherical distribution of diffusion axis with respect to the magnetic field.

When a bilayer is perfectly aligned, a single sharp resonance is expected at a chemical shift $\delta = \delta_{iso} + 1/3\Delta\delta(3\cos^2\theta - 1)$ where θ is the angle between the bilayer normal and the B_0 field (e.g., Figure 4b, $\theta = 90°$). The resonance is symmetric and its half-height width Δ is dictated ideally by its T_2 relaxation time.

Experimentally, in the oriented L_α liquid crystalline membrane, each resonance may be broadened by various mechanisms (for dilute I = 1/2 nuclei like carbon 13): Local magnetic field inhomogeneities can occur over the sample volume or over the experiment time. This is classically coped with in liquid state NMR by using careful shimming on a sample resonance and lock, but is rarely done on oriented membrane samples.

Imperfections in the orientation of the lipids are manifested in the NMR spectra in several ways. If part of the sample is not perfectly aligned, two major kinds of resonance frequency distribution may be observed: first, if part of the sample has a spherical distribution of orientations (due to the presence of liposomes), powder pattern components appear in the spectrum (Figure 4a–c); secondly, a distribution of

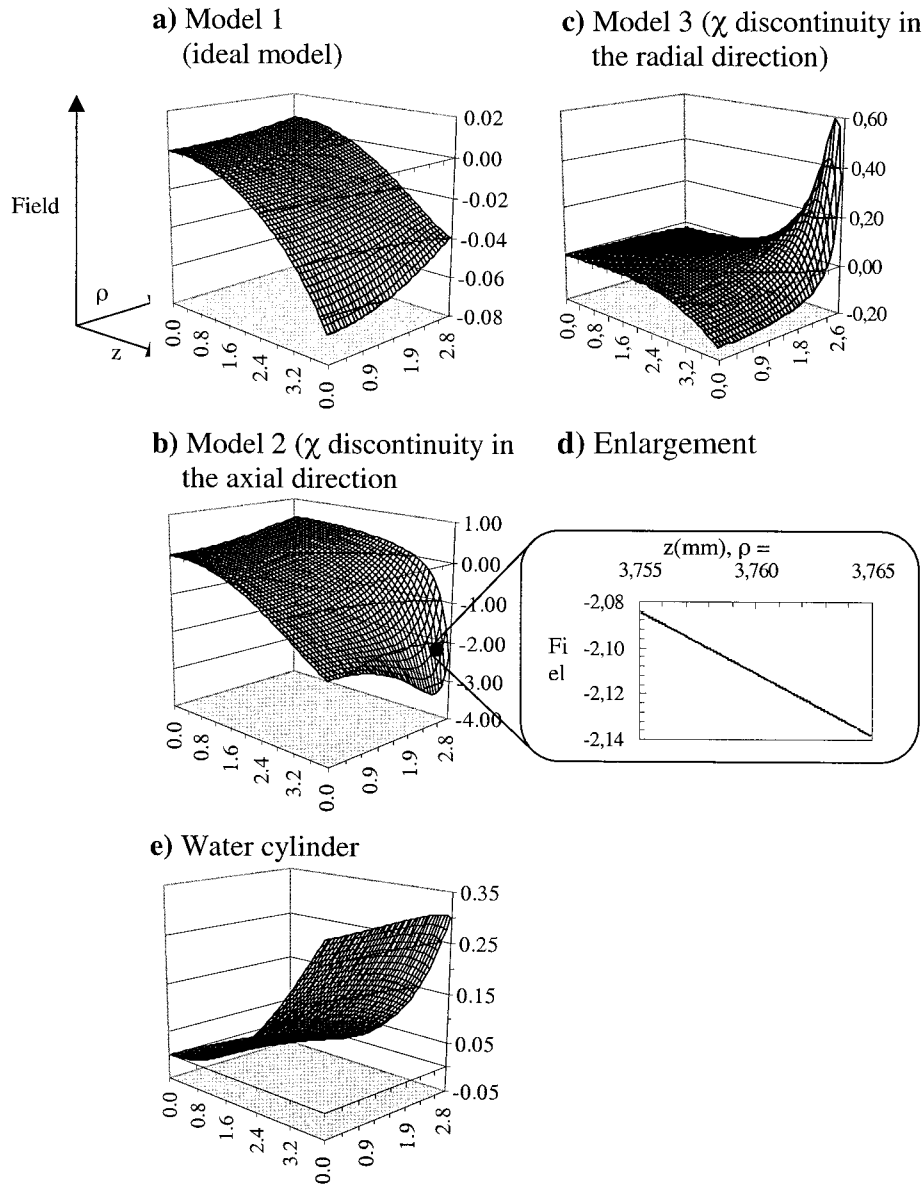

Figure 3. Induced magnetic field shape. (a)–(c) Variations of the relative induced magnetic field intensity $(B_{ind}\text{-}B_{ind,c})/B_0 \times 10^6$ (noted as Field in the axis definition) as a function of radial ρ (in mm) and axial z (in mm) directions, for model 1 to 3 (see Figure 2 legend for model definitions). Positions in z directions are taken in the middle of each lipid layer. $B_{ind,c}$ are the values of the induced field obtained at the centre of the sample stacking. φ was set to 0°. (d) Variation of $(B_{ind}\text{-}B_{ind,c})/B_0 \times 10^6$ within one lipid multi-layers, 10 μm around z = 3.76 mm, at ρ = 2.61 mm. (e) Variations of $(B_{ind}\text{-}B_{ind,c})/B_0 \times 10^6$ along a cylinder filled with water.

bilayer normal around the mean rotational axis, can exist. Then, as often described in previous papers, a Gaussian distribution of orientations is employed to simulate the system, and the 'mosaic spread' is defined by the standard deviation σ of the Gaussian curve. Figures 4d and 4e display the line shapes of a resonance as a function of the chemical shift anisotropy for sample with their bilayer normal perpendicular to the magnetic field (Figure 4d) or aligned with the magic Angle (4e). Mosaic spread σ has been chosen equal to $\pm 2°$ and two typical values of CSA were selected ($\Delta\delta = 2$ and 20 ppm). It is shown in Figure 4d that at 90° (and also at 0°, data not shown) the contribution of mosaic spread to the linewidth remains weak as long

as the mosaic spread and $\Delta\delta$ are kept reasonable. This is expected from the dependence of δ on θ since the first derivative ($\partial\delta/\partial\theta = 2\Delta\delta\cos\theta\sin\theta$) is equal to 0 both at 0° and 90°. This is not true at the magic angle and it is shown on Figure 4e that then the effect of mosaic spread can be quite large. As a rule of thumb, simulations show that one can expect a line broadening of about 0.04 ppm per $\Delta\delta$ ppm unit, per degree of mosaic spread σ at the magic angle. The same simulations were performed for typical experiments with ^{15}N labelled peptides and bilayers oriented at 0°, i.e., with a CSA $\Delta\delta = 170$ ppm and a T_2 dominated linewidth of 1.5 ppm. The linewidths obtained assuming mosaic spread values of $\pm 1°$, $\pm 2°$, $\pm 3°$, $\pm 5°$, $\pm 10°$ were 1.6, 1.9, 2.4, 4.1, and 11 ppm, respectively, showing that, in this case also, peptide's mosaic spread values of 5° and above may dominate the final linewidths.

Mosaic spread measurement from linewidth at the magic angle

In the literature, a wide range of values for mosaic spread (from 0.1° to 30°) has been reported for pure DMPC bilayer using neutron or x-ray diffraction depending on the experimental conditions. NMR has also been used for characterising the mosaic spread on membranes either by analysing the line shape at 0° orientation or by comparing the ^{31}P linewidth at several angles. Values generally described range from 1° to 4° (Glaubitz and Watts, 1998). One general problem is to take into account the contribution of B_0 field inhomogeneities. In order to overcome this difficulty and to access an accurate mosaic spread measurement we used several resonances displaying different CSA and/or two orientations. Since the mosaic spread effect is highly dependant on the CSA values (Figure 4e) and on the bilayer orientation (Figures 4d and 4e), one can separate the contribution to linewidth of B_0 field inhomogeneities from that of mosaic spread.

We used herein bilayers of DMPC-[$\gamma-^{13}C$]/$^{13}C_4$-cholesterol with their membrane normal oriented at the magic angle and compared the carbon linewidth of both choline methyl (CSA $\Delta\delta = 2$ ppm) and cholesterol C_4 (CSA $\Delta\delta = 20$ ppm). The lipid surface density (i.e., 1 mg/cm^2) and the experimental protocol used allowed us to have a negligible contribution of liposomes as shown by the ^{31}P spectra (data not shown). The sample was placed in a 5-mm MAS rotor at the magic angle in the MAS probe. Careful shimming was performed on the proton choline methyl signal in rotating conditions (2 kHz) for B_0 field inhomogeneities along the rotation axis and on the choline carbon resonance without rotation for inhomogeneities perpendicular to the magic angle axis in a way similar to liquid state shimming. Best static linewidths thus obtainable were 0.24 ± 0.02 ppm for choline methyl and 0.36 ± 0.03 ppm for cholesterol C_4 resonances. These values are still larger than expected from T_2 measurements (respectively 0.096 ppm and

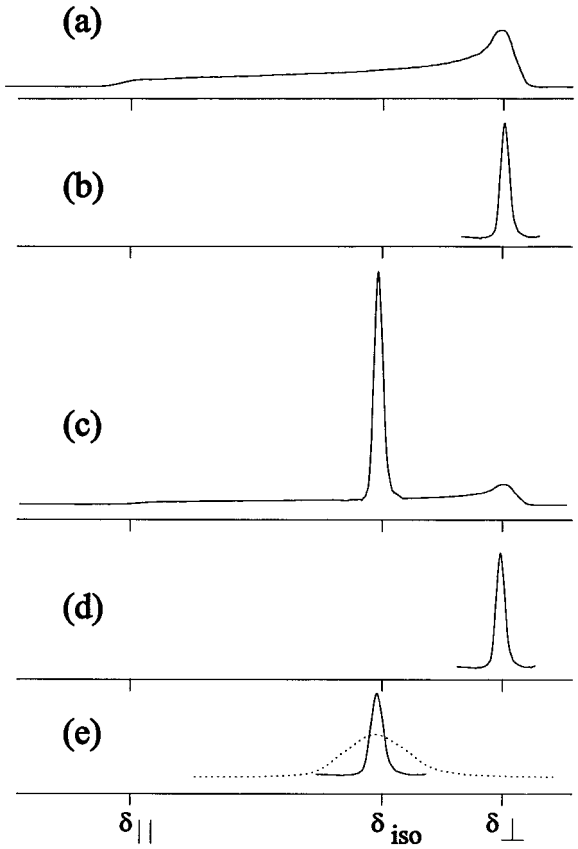

Figure 4. Spectral simulations illustrating the various sources of line broadening for an axially symmetric tensor. The intrinsic linewidth ($1/\pi T_2$) was set to 0.21 ppm. Two cases of CSA were examined, a CSA of 2 ppm (choline methyl) and a CSA of 20 ppm (cholesterol C_4). (a) Powder pattern representative of a spherical distribution of membrane orientations (CSA = 20 ppm), as observed typically with liposomes. (b) Perfectly oriented sample with the bilayer normal perpendicular to the magnetic field; the linewidth is dictated entirely by T_2. (c) Bilayers oriented at the magic angle, with a significant contribution of unoriented liposomes (50%). It is mainly visible by the shoulder at $\delta_\perp$. (d) The distribution of intensity expected for a resonance characterised by a CSA of 2 ppm (filled line) or 20 ppm (dotted line, not visible here) and a Gaussian distribution of orientations centred at 90° with a standard deviation $\sigma = 2°$ ('mosaic spread' of $\pm 2°$). (e) Same as (d) but for bilayers oriented at Magic Angle. The increase in linewidth for large CSA value (20 ppm, dotted line) is now clearly visible, illustrating that mosaic spread effects are more pronounced at MA than at 90°.

0.14 ppm, Table 1) and cannot be fitted by the sole contribution of mosaic spread. Since they were measured on the same spectrum, i.e., same sample and same experimental conditions, they must be accounted for by one single set of B_0 field inhomogeneities and sample mosaic spread. Line shapes were simulated by assuming a Gaussian distribution of B_0 values (standard deviation σ', resulting B_0 broadened line of half height linewidth Δ') and a Gaussian distribution of orientations (standard distribution σ) as described in Material and methods section. The experimental spectrum could be best simulated by a single pair of values $\sigma' = 9 \pm 1$ Hz (producing Δ' values of 0.22 ppm for choline and 0.26 ppm for cholesterol) and $\sigma = 0.30° \pm 0.05°$. In order to crosscheck this result, we also used the ^{31}P resonance ($\Delta\delta = 48 \pm 2$ ppm, $1/\pi T_2 = 0.55 \pm 0.03$ ppm, Table 1). On the same sample we observed a linewidth of 0.94 ± 0.03 ppm, also compatible with our estimation of residual magnetic field effect ($\Delta' = 0.57$ ppm) and mosaic spread measurement.

It should be noted that both effects contribute to the observed linewidth even after careful shimming on the sample and that neglecting B_0 field inhomogeneities effects may lead to an overestimation of mosaic spread whenever σ' is not much smaller than $1/\pi T_2$. This is why it is necessary to measure two separate resonances on the same sample. One of them, such as the choline methyl resonance, should have a small CSA for good shimming and estimation of σ; the other one must have a large CSA and be measured at the magic angle, to be highly influenced by mosaic spread (such as cholesterol C_4 or the ^{31}P resonance).

Shimming an oriented bilayer using an internal reference

From the typical experimental linewidth observed for cholesterol C_4 carbon resonance (≈ 1.5 ppm) and the mosaic spread determined above it is clear (Figure 4d) that mosaic spread is not a significant parameter affecting linewidth when the bilayer normal is perpendicular to the magnetic field director. A mosaic spread of $\pm 0.30°$ only increases the cholesterol C_4 linewidth from 0.21 ppm to 0.23 ppm. Therefore, much more attention must be paid to shimming than previously done. Classically, shims are optimised on a sample of water and are directly applied to the sample of interest, whereas proper shimming should be performed on an internal signal such as the solvent resonance. The problem of oriented bilayers samples is generally the lack of an intense, sharp resonance for shimming. Hydration water could appear as a good candidate and indeed we have seen before that one can shim a sample of water between glass plates. However, membrane samples are weakly hydrated and the water remains highly anisotropic as seen from quadrupole splitting in deuterium NMR (Faure et al., 1997), and neither D_2O nor H_2O could be used for shimming. Deuterated γ-methyl of DMPC choline could not be used either due to its short T_2 (for a DMPC/30 mol% cholesterol at 313 K, we observed a quadrupole splitting of 950 ± 50 Hz and a linewidth of ≈ 1.6 ppm). Another idea was to incorporate a small amount of TMS (tetramethyl silane) which could be assumed to undergo isotropic diffusion because of its nearly spherical shape. Again its ^1H resonance was too broad for shimming (≈ 3 ppm). From Table 1, it is clear that the choline methyl carbon resonance is a suitable candidate being sharp ($1/\pi T_{2\perp} = 0.12$ ppm, due to the choline headgroup high dynamic), intense (3 equivalent methyl), and having a very small CSA (2 ppm) so that mosaic spread broadening will be negligible in most samples and orientations. Also choline containing lipids are present in most model membranes whereas cholesterol may not be present. Finally, head group carbon 13 labelled DMPC is easily obtained by permethylation of DMPE with $^{13}CH_3I$ (see Materials and methods section).

Using a typical sample containing 8-9 mg $^{13}C_\gamma$-DMPC, and single pulse experiment (or CP with a long contact time, 2–5 ms), one can get an intense choline signal in one scan and shim on this signal. Figure 5 illustrates the significant resolution and sensitivity improvement obtained in using this approach. The major signals are due to the choline methyl at 55 ppm (taken as an internal reference of chemical shift), the cholesterol C_4 at 49.9 ppm and the unresolved phospholipid methylene at 39 ppm. Here, cholesterol C_4 resonance is narrowed down to 0.3 ppm. Such a carbon resolution has never been observed before on glass plates oriented membrane sample and is close to the limit of the transverse relaxation time (0.21 ppm). Natural abundance phospholipid polar head group signals are also visible from 50 to 70 ppm. Note also that several methyl are well resolved at 10–35 ppm together with the two acyl carbonyls at 162 ppm (sn_1) and 175 ppm (sn_2). Expansions in Figure 5b show that the resolution enhancement allows us to have access to several long range carbon-phosphorus dipolar couplings which had been solely measured before using DMPC oriented in bicelles (Sanders, 1993)

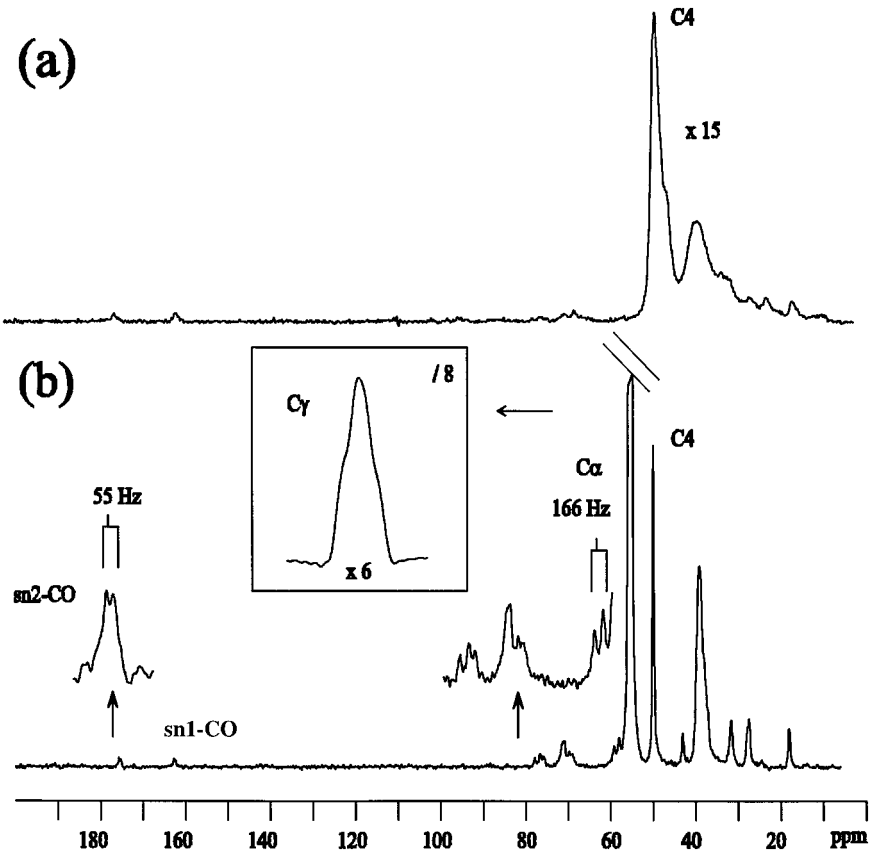

Figure 5. DMPC/$^{13}C_4$-cholesterol lipid bilayer oriented at 90°: (a) Typical ^{13}C spectrum obtained after shimming on a water sample tube (taken from Massou et al. (1999)). (b) 1D ^{13}C CP spectrum obtained with $13C_\gamma$-labelled choline, after shimming on the choline carbon resonance. (8.1 mg $^{13}C_\gamma$-DMPC, 1.4 mg $^{13}C_4$-cholesterol, 2.5 ms CP contact time, temperature 313K). The best cholesterol C_4 linewidth thus obtained was 0.3 ppm. The choline C_γ resonance is the most intense resonance in the spectrum and is shown at a smaller intensity and higher chemical shift scale in the square box. Note that it is broader due to an internal structure. The gain in resolution is of course accompanied with an important gain in sensitivity, while keeping the full anisotropic information. The chemical shifts of the two resolved carbonyl are equal to 162 ppm (sn_1) and 175 ppm (sn_2).

or by MAS experiment in using recoupling (Hong et al., 1995a,b). For instance, CO-sn_2 and choline C_α (58.5 ppm) are observed as doublets with dipolar splitting equal to 55 Hz and 166 Hz respectively. The resolution obtained here is close to the resolution in isotropic spectra resulting from MAS experiments. The gain in resolution (and sensitivity) demonstrated here, while keeping the full anisotropic information will be extremely useful in the extraction of orientational constraints from 1D and 2D experiments with specifically and uniformly ^{13}C labelled peptides, although in the later case, assignment strategies need to be further developed. It should be noted also that for some peptides, their mosaic spread was found to be higher than the lipid's one in the same sample and thus may be the limiting factor in the final resolution (see end of Conclusions).

2D PELF experiment

As an example of the possibilities offered by high resolution oriented bilayer spectra, a 2D PELF experiment was performed. This experiment, initially developed on oriented liquid crystals (Caldarelli et al., 1996) correlates the carbon chemical shift with carbon – proton dipolar couplings which can be used to analyse the conformation, orientation and dynamics of the molecule of interest. Figure 6 shows the result of this experiment on our DMPC/cholesterol oriented lipid bilayer. Two dipolar splitting constants can clearly be resolved for the cholesterol C_4 resonance (5.3 kHz and 7.5 kHz), and can be assigned

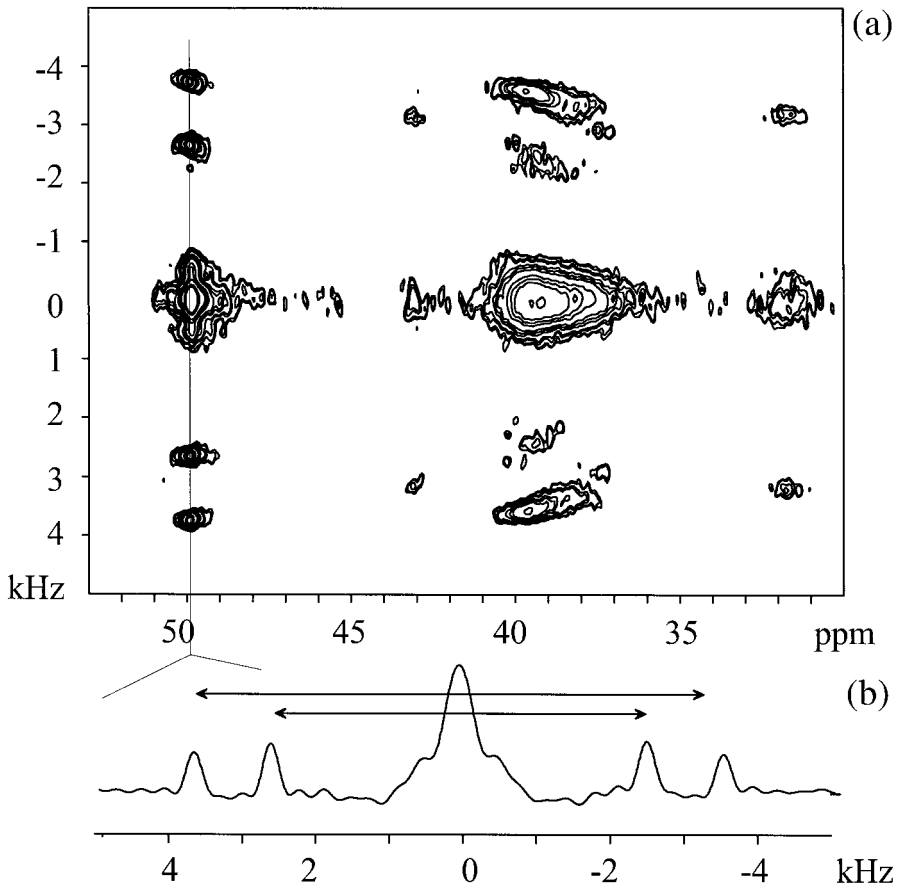

Figure 6. 2D PELF experiment (same sample as in Figure 5b). (a) Contour plot of the PELF spectra. (b) Slice through the cholesterol C_4 resonance. The dipolar scale has been corrected by the 0.47 MREV-8 scaling factor.

to the dipolar (plus scalar) couplings of C_4 with the equatorial and axial H_4 protons respectively (Massou et al., 1999). These values are in good agreement with previous analysis of this sample using deuterium NMR (Marsan et al., 1999). Some other dipolar couplings are clearly resolved on the 2D PELF: they can be tentatively assigned to the acyl chain methylene C_2 (43 ppm), to the other non resolved methylenes (38–40 ppm) and to a cholesterol methyl (32 ppm). It is clear that the gain in resolution and sensitivity opens the way to use this experiment on uniformly labelled sterols in order to determine their orientation and dynamics from one single 2D experiment.

Fine structure of the choline methyl carbon resonance

In our experimental conditions, the choline methyl signal could not be narrowed down further than 0.7 ppm while the cholesterol resonance had linewidth of 0.3 ppm. At a high level of resolution enhancement, (see inset) the γ-methyl appears to display an internal fine structure. In this experiment, ^{13}C-^{1}H dipolar couplings are effectively removed by proton decoupling. However other dipolar couplings remain (although being partially averaged by the fast axial diffusion of all the molecules along the bilayer normal), such as ^{13}C-^{13}C and ^{13}C-^{31}P dipolar couplings. These are expected to occur in particular between the three methyl carbons of choline. In order to confirm their existence, and to determine them more accurately, we performed a 'D-resolved' experiment. Apart from continuous ^{1}H TPPM decoupling and the initial cross polarisation period, the pulse sequence was identical to the J-resolved liquid state experiment (Aue et al., 1976). After cross polarisation from ^{1}H, the ^{13}C magnetisation evolves under the ^{13}C-^{13}C homonuclear dipolar coupling alone, since both the ^{13}C-^{31}P and the chemical shift interactions (including B_0 field inhomogeneity effects) are removed by the 180° pulse in the middle of the evolution period. The ^{13}C magnetisation

is then directly detected under ^{1}H decoupling. After standard tilt and symmetrisation one gets a 2D spectrum with pure ^{13}C-^{13}C dipolar coupling evolution in F1 and ^{13}C chemical shift with ^{31}P-^{13}C dipolar couplings in F2. In Figure 7a are compared the line shapes obtained from a single pulse experiment for choline methyl (7a) and rows extracted from the D-resolved experiment for choline methyl (7b) and cholesterol C_4 carbons (7c). The difference between the linewidth of choline methyl and cholesterol C_4 extracted from the 2D experiment can be attributed to the choline ^{31}P-^{13}C dipolar interaction. When the data are corrected for the small contribution of the mosaic spread, the difference can be simulated with a value of $D_{P-C} = 15 \pm 3$ Hz, which is close to the value suggested by Sanders for a pure DMPC L_α phase (Sanders, 1993). Note that no contribution from scalar/dipolar ^{13}C-^{14}N coupling and from differential line broadening effect have been used in the simulation (Oldfield et al., 1991). Figure 7d displays the F1 column corresponding to choline methyl chemical shift. As expected, the ^{13}C-^{13}C dipolar coupling between the three equivalent carbons of the choline methyl group gives rise to a triplet with a splitting value of 35 Hz ± 3 Hz. The spectrum 7e is the simulated line shape obtained with the preceding parameters, i.e., apparent linewidth $\Delta' = 0.3$ ppm, homonuclear (C-C, 35 Hz) and heteronuclear (C-P, 15 Hz) dipolar couplings. The line shape is found to be in good agreement with the single pulse line shape displayed in Figure 7a. This experiment shows that a very high resolution can be obtained on oriented bilayers, both with a highly oriented sample ($\sigma = \pm 0.30°$) and with direct shimming on this sample; it allows to directly measure dipolar couplings as small as 10 Hz.

As a final remark, we should stress that the choline methyl signal, which proved to be very useful for shimming, may not be however the optimum candidate due to this homonuclear C – C coupling. One could use instead DMPC labelled on one single carbon, the carbonyl on the sn1 chain which appears to be sharp enough (Figure 5b), or one of the methyl carbons at the end of the acyl chain (0.12–0.16 ppm expected linewidth from MAS experiments on liposomes).

Conclusions

In the present work we have determined quantitatively, both through simulations and experiments, the relative contributions of several parameters affecting the resolution on carbon 13 spectra of oriented bilayers.

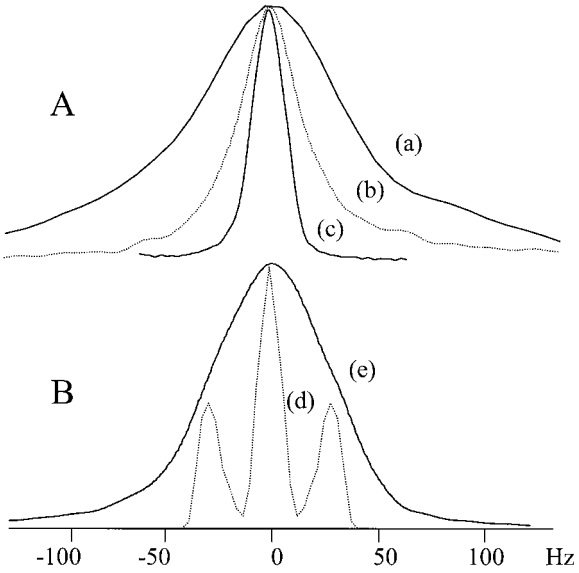

Figure 7. 2D 'D-resolved' experiment (same sample as in Figure 5b). Apart from ^{1}H TPPM decoupling during t_1 and t_2, and the initial cross polarisation period, the pulse sequence was identical to the homonuclear J-resolved liquid state experiment (Aue et al., 1976). (a) Line shape of the choline methyl resonance in a 1D ^{1}H decoupled ^{13}C spectrum. (b) Cross section of the 'D-resolved' experiment at $\omega 1 = 0$ Hz (dotted line), corresponding to the choline methyl resonance (55 ppm). (c) Cross section of the 'D-resolved' experiment at $\omega 1 = 0$ Hz, corresponding to the cholesterol C_4 resonance (49.9 ppm). (d) Cross section along $\omega 1$ at $\omega 2 = 55$ ppm, i.e. carbon-carbon dipolar couplings of the choline methyl resonance. A splitting of 35 Hz can be directly measured on the spectrum. (e) Simulated spectrum of the choline methyl carbon resonance taking into account an apparent linewidth $\Delta' = 0.24$ ppm ($\sigma' = 8.6$ Hz, $\Delta'^{13}C_4 = 0.3$ ppm), ^{13}C-^{31}P dipolar coupling (15 Hz) and ^{13}C-^{13}C dipolar coupling (35 Hz).

An optimum way to quantify field inhomogeneities and mosaic spread is to measure the linewidth of the choline methyl carbon resonance (influenced mainly by shims) and the ^{31}P resonance (heavily influenced by mosaic spread) on the same sample at the magic angle. It appears that for bilayers oriented at the magic angle mosaic spread can play a significant role on linewidths. At 90° and 0° orientations however, the major parameter is B_0 field inhomogeneities and careful shimming on an internal signal is necessary to obtain the highest resolution. After doing so linewidth of 0.2–0.3 ppm can be obtained for carbon resonances in membranes in the fluid phase, a resolution which opens the way to a variety of 2D experiments using uniformly labelled molecules. The 2D PELF experiment provides ^{13}C-H dipolar couplings for each resolved carbon resonance, while the 2D D-resolved experiment can be used to measure accurately ^{13}C-^{13}C

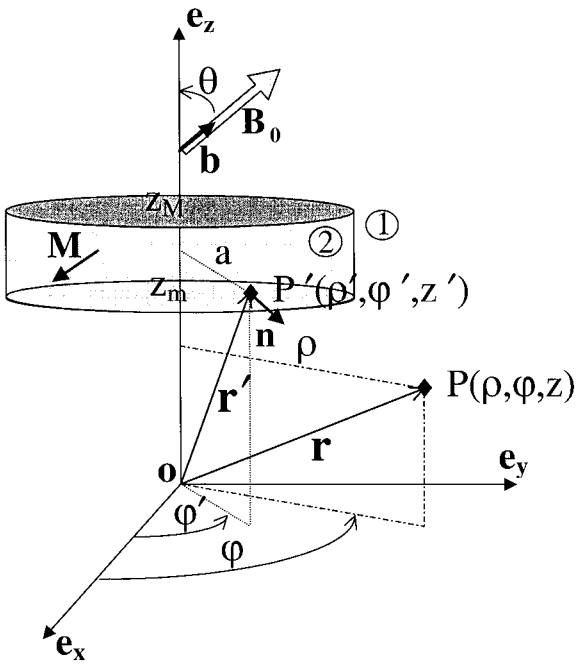

Figure 8. Schematic representation of the coordinates system for the calculation of induced magnetic field created by a cylindrical material (radius = a, thickness = $z_M - z_m$). Magnetisation M and homogeneous external field B_0 lay along the unit vector b defined by the θ angle from the cylindrical axis. n is the unit vector normal to the surface (lateral and facial) at the point $P'(r')$. The total induced magnetic field $B_{ind}(r)$ is calculated at the position defined by P(r).

dipolar couplings in a uniformly labelled molecule and thus extract numerous orientational constraints.

Thus shimming directly on a sample resonance is required to get the highest resolution on oriented bilayer ^{13}C spectra of lipids. It should be stressed at this point that we have been using a DMPC/cholesterol sample in the fluid phase which is known to orient particularly well, in agreement with the 0.3° mosaic spread found herein, and that the carbon resonances observed have sharp intrinsic linewidths (< 0.2 ppm). The situation may be very different for peptide-membrane samples. First, it should be noted that all our analyses were performed in the assumption that the bilayer normal is a fast diffusion axis for all molecules, which is valid for cholesterol in DMPC, but is not true for many peptides/proteins. The treatment of mosaic spread effect is very different in the rigid body hypothesis (Nevzorov et al., 1999). The typical T_2-dominated linewidths of peptides and proteins in membranes are often higher than 1 ppm (Marassi et al., 1997; Song et al., 2000). Peptides/proteins mosaic spreads are often in a 5–20 degrees range, which combined with a ^{15}N CSA of about 170 ppm makes it a dominant parameter. In some cases, lipids and peptides even display a different mosaic spread within the same sample (Bechinger et al., 1993; Glaubitz et al., 1999; Grobner et al., 1998; Middleton et al., 2000; Williamson et al., 1998). With all these restrictions in mind, it may nevertheless be useful to pay more attention to shims whenever the T_2 dominated linewidths are smaller than 1 ppm.

Acknowledgements

The NMR equipment has been financed by the CNRS (Dept. SdV and programme IMABIO) and the region Midi-pyrénées.

Appendix A

The general expression of the magnetic field induced by any material of magnetic susceptibility χ subject to a strong magnetic field B_0 is:

$$\mathbf{B_{eff}}(\mathbf{r}) = \frac{\mu_0}{4\pi}\left[\iint d^2r' \frac{\mathbf{J}(\mathbf{r}') \wedge (\mathbf{r}-\mathbf{r}')}{(\mathbf{r}-\mathbf{r}')^{3/2}} + \iiint d^3r' \frac{\mathbf{S}(\mathbf{r}') \wedge (\mathbf{r}-\mathbf{r}')}{(\mathbf{r}-\mathbf{r}')^{3/2}}\right].$$

Here $\mathbf{J}(\mathbf{r}') = \mathbf{M} \wedge \mathbf{n}(\mathbf{r}')$ and $\mathbf{S}(\mathbf{r}') = \nabla \wedge \mathbf{M}$ are the equivalent surface current and the equivalent volumic current, respectively. $\mathbf{n}$ represents the unit normal vector to the surface (Figure 8), $\mathbf{M} = \frac{\chi_2 \mathbf{B}}{\mu_0(1-\chi_2)} - \frac{\chi_1 \mathbf{B}}{\mu_0(1-\chi_1)}$ is the magnetization per unit volume where χ_2 and χ_1 correspond to the magnetic susceptibility inside and outside the material, respectively. Since $\mathbf{M}$ is supposed to be uniform inside and outside the material - $\mathbf{S}(\mathbf{r}') = 0$, and $\chi \ll 1$ - local effects of $\mathbf{M}$ on $\mathbf{B_0}$ can be neglected and $\mathbf{M}$ expressed as $\mathbf{M} = (\chi_2 - \chi_1)\mathbf{B_0}/\mu_0$. Thus, the calculation of the induced field only requires the evaluation of the following expression

$$\mathbf{B_{ind}}(\mathbf{r}) = \frac{\mu_0}{4\pi}\iint \mathbf{d^2r'} \frac{\mathbf{J}(\mathbf{r}') \wedge (\mathbf{r}-\mathbf{r}')}{(\mathbf{r}-\mathbf{r}')^{3/2}}.$$

For cylindrical geometry (Figure 8), the unit normal vector $\mathbf{n}$ lies on three distinct regions: the lateral surface and the two faces at the top and bottom cuts. The expression of the lateral and facial surface currents when written in cylindrical coordinates are

$$\mathbf{J^1} = \left[\cos\theta(\sin\varphi'\mathbf{e_x} + \cos\varphi'\mathbf{e_y}) - \sin\theta\cos\varphi'\mathbf{e_z}\right](\chi_2 - \chi_1)B_0/\mu_0$$

and

$$\mathbf{J^f} = [\pm \sin\theta.\mathbf{e_z}](\chi_2 - \chi_1)B_0/\mu_0$$

where $(+)$ is used for the top face and $(-)$ for the bottom face (see Figure 8 for axis convention).

In high-field NMR, one is interested in the component of the induced field along the large polarizing field B_0 direction (defined by $\mathbf{b}$) since this gives the major effect on the nuclear spin precession frequency. Furthermore, the lateral and facial surface integrals can be written as an integral over z' and φ' and over ρ' and φ', respectively. The integrations over z' and ρ' were performed analytically, leaving for each surface integral a one-dimensional numerical integration over the azimuthal angle.

The induced field created by the lateral surface at the position P(ρ,φ,z) is

$$B^1_{ind}(\rho, \varphi, z) = \mathbf{B^1_{ind}} \cdot \mathbf{b}$$

$$B^1_{ind}(\rho, \varphi, z) = \frac{(\chi_2 - \chi_1)B_0}{4\pi} \int_0^{2\pi}\int_{z_m}^{z_M} \frac{\sin\varphi'\cos\theta(z-z')\sin\theta - \cos\varphi'\sin^2\theta(\rho\cos\varphi - a\cos\varphi') + \cos^2\theta(a - \rho\cos(\varphi'-\varphi))}{\left[\rho^2 + a^2 - \rho a\cos(\varphi'-\varphi) + (z-z')^2\right]^{3/2}} adz'd\varphi'$$

and analytical integration over z axis

$$B^1_{ind}(\rho, \varphi, z) = \frac{(\chi_2 - \chi_1)B_0}{4\pi}\int_0^{2\pi}\{A_1 + A_2 + A_3(A_4 - A_5)\}\, d\varphi'$$

with

$$A_1 = \frac{a\sin\varphi'\cos\theta\sin\theta}{\sqrt{\rho^2 + a^2 - \rho a\cos(\varphi'-\varphi) + (z - z_M)^2}}$$

$$A_2 = \frac{a\sin\varphi'\cos\theta\sin\theta}{\sqrt{\rho^2 + a^2 - \rho a\cos(\varphi'-\varphi) + (z - z_m)^2}}$$

$$A_3 = \frac{a\left(\cos^2\theta\left(a-\rho\cos\left(\varphi'-\varphi\right)\right)-\sin^2\theta\cos\varphi'\left(\rho\cos\varphi-a\cos\varphi'\right)\right)}{\rho^2+a^2-\rho a\cos\left(\varphi'-\varphi\right)+\left(z-z_M\right)^2}$$

$$A_4 = \frac{z-z_m}{\sqrt{\rho^2+a^2-\rho a\cos\left(\varphi'-\varphi\right)+\left(z-z_m\right)^2}}$$

$$A_5 = \frac{z-z_M}{\sqrt{\rho^2+a^2-\rho a\cos\left(\varphi'-\varphi\right)+\left(z-z_M\right)^2}}.$$

The two facial induced fields produced by plate at the position P(ρ,φ,z) on the top and the bottom faces are

$$B_{ind}^{fz_m}(\rho,\varphi,z) = \mathbf{B_{ind}^{fz_m}}\cdot\mathbf{b}$$

$$B_{ind}^{fz_m}(\rho,\varphi,z) = \frac{(\chi_2-\chi_1)B_0}{4\pi}\int_0^{2\pi}\int_0^{a}\frac{\sin^2\theta(z-z_m)-\sin\theta\cos\theta(\rho\sin\varphi-\rho'\sin\varphi')}{\left[\rho^2+\rho'^2-\rho\rho'\cos(\varphi'-\varphi)+(z-z_m)^2\right]^{3/2}}\rho' d\rho' d\varphi'$$

and

$$B_{ind}^{fz_M}(\rho,\varphi,z) = -B_{ind}^{fz_m}(\rho,\varphi,z).$$

After analytical integration over ρ′, B_{ind}^{fzm} can be written as

$$B_{ind}^{fzm}(\rho,\varphi,z) = \frac{(\chi_2-\chi_1)B_0}{4\pi}\int_0^{2\pi}\{B_1B_2+B_3(B_4+B_5+B_6)\}\,d\varphi'$$

with

$$B_1 = \frac{\sin^2\theta\,(z-z_m)-\rho\sin\theta\cos\theta\sin\varphi}{\rho^2\sin^2\left(\varphi'-\varphi\right)+\left(z-z_m\right)^2}$$

$$B_2 = \sqrt{\rho^2+(z-z_m)^2}-\frac{\rho^2+(z-z_m)^2-\rho a\cos\left(\varphi'-\varphi\right)}{\sqrt{\rho^2+a^2-\rho a\cos\left(\varphi'-\varphi\right)+\left(z-z_m\right)^2}}$$

$$B_3 = \sin\theta\cos\theta\sin\varphi'$$

$$B_4 = \frac{\rho\cos\left(\varphi'-\varphi\right)\sqrt{\rho^2+(z-z_m)^2}}{\rho^2\sin^2\left(\varphi'-\varphi\right)+\left(z-z_m\right)^2}$$

$$B_5 = \frac{2\rho^2 a\cos^2\left(\varphi'-\varphi\right)-\left(a+\rho\cos\left(\varphi'-\varphi\right)\right)\left(\rho^2+(z-z_m)^2\right)}{\left(\rho^2\sin^2\left(\varphi'-\varphi\right)+\left(z-z_m\right)^2\right)\sqrt{\rho^2+a^2-\rho a\cos\left(\varphi'-\varphi\right)+\left(z-z_m\right)^2}}$$

$$B_6 = \ln\frac{\sqrt{\rho^2+a^2-\rho a\cos\left(\varphi'-\varphi\right)+\left(z-z_m\right)^2}+a-\rho\cos\left(\varphi'-\varphi\right)}{\sqrt{\rho^2+\left(z-z_m\right)^2\rho\cos\left(\varphi'-\varphi\right)}}.$$

Numerical integrations over φ′ are performed using Romberg techniques, with a convergence threshold of 10^{-8}.

The induced field coming from every interfaces of the model (Figure 8) can be calculated from one of these three expressions depending on its orientation. The total induced magnetic field B_{ind} at different position in the sample bilayers is then obtained by the summation over every surface contributions.

References

Aue, W.P., Karhan, J. and Ernst, R.R. (1976) *J. Chem. Phys.*, **64**, 4226–4227.

Barbara, T.M. (1994) *J. Magn. Reson.*, **58**, 413–420.

Bechinger, B., Zasloff, M. and Opella, S.J. (1993) *Protein Sci.*, **2**, 2077–2084.

Bennet, A.E., Riensta, C.E., Auger, M.M., Lakshmi, K.V. and Griffin, R.G. (1995) *J. Chem. Phys.*, **103**, 6951–6958.

Bersch, B., Starck, J.P., Milon, A., Nakatani, Y. and Ourisson, G. (1993) *Bull. Soc. Chim. Fr.*, **130**, 575–583.

Caldarelli, S., Hong, M., Emsley, L. and Pines, A. (1996) *J. Phys. Chem.*, **100**, 18696–18701.

Cross, T.A. (1997) *Meth. Enzymol.*, **289**, 672–696.

Doty, F.D., Entzminger, G. and Yang, Y.A. (1998) *Concept. Magn. Reson.*, **10**, 133–156.

Dufourc, E.J., Mayer, C., Stohrer, J., Althoff, G. and Kothe, G. (1992) *Biophys. J.*, **61**, 42–57.

Dufourc, E.J., Parish, E.J., Chitrakorn, S. and Smith, I.C.P. (1984) *Biochemistry*, **23**, 6062–6071.

Faure, C., Bonakdar, L. and Dufourc, E.J. (1997) *FEBS Lett.*, **405**, 263–266.

Glaubitz, C. and Watts, A. (1998) *J. Magn. Reson.*, **130**, 305–316.

Glaubitz, C., Burnett, I.J., Gröbner, G., Mason, J. and Watts, A. (1999) *J. Am. Chem. Soc.*, **121**, 5787–5794.

Grobner, G., Choi, G., Burnett, I.J., Glaubitz, C., Verdegem, P.J., Lugtenburg, J. and Watts, A. (1998) *FEBS Lett.*, **422**, 201–204.

Herzfeld, J. and Chen, X. (1996) In Grant, D.M. and Harris, R.K. (eds), *Encyclopedia of NMR*, Vol. 7, John Wiley & Sons Ltd., pp. 4362–4369.

Hong, M., Schmidt-Rohr, K. and Nanz, D. (1995a) *Biophys. J.*, **69**, 1939–1950.

Hong, M., Schmidt-Rohr, K. and Pines, A. (1995b) *J. Am. Chem. Soc.*, **117**, 3310–3311.

Marassi, F.M., Ramamoorthy, A. and Opella, S.J. (1997) *Proc. Natl. Acad. Sci. USA*, **94**, 8551–8556.

Marsan, M.P., Muller, I., Ramos, C., Rodriguez, F., Dufourc, E.J., Czaplicki, J. and Milon, A. (1999) *Biophys. J.*, **76**, 351–359.

Massou, S., Tropis, M. and Milon, A. (1999) *J. Chim. Phys.*, **96**, 1595–1601.

Middleton, D.A., Rankin, S., Esmann, M. and Watts, A. (2000) *Proc. Natl. Acad. Sci. USA*, **97**, 13602–13607.

Nevzorov, A.A., Moltke, S., Heyn, M.P. and Brown, M.F. (1999) *J. Am. Chem. Soc.*, **121**, 7636–7643.

Oldfield, E., Adebodun, F., Chung, J., Montez, B., Park, K.D., Le, H.B. and Phillips, B. (1991) *Biochemistry*, **30**, 11025–11028.

Sanders, C.R. (1993) *Biophys. J.*, **64**, 171–181.

Seelig, J., Gally, G.U. and Wohlgemuth, R. (1977) *Biochim. Biophys. Acta*, **467**, 109–119.

Separovic, F., Gehrmann, J., Milne, T., Cornell, B.A., Lin, S.Y. and Smith, R. (1994) *Biophys. J.*, **67**, 1495–1500.

Song, Z., Kovacs, F.A., Wang, J., Denny, J.K., Shekar, S.C., Quine, J.R. and Cross, T.A. (2000) *Biophys. J.*, **79**, 767–775.

Watnick, P.I. (1990) *Proc. Natl. Acad. Sci. USA*, **87**, 2082–2086.

Williamson, P.T., Grobner, G., Spooner, P.J., Miller, K.W. and Watts, A. (1998) *Biochemistry*, **37**, 10854–10859.